ACS APPLIED MATERIALS & INTERFACES

Research Article

www.acsami.org

Epitaxial Growth Route to Crystalline TiO_2 Nanobelts with Optimizable Electrochemical Performance

Peng Gao,*[,†] Di Bao,[†] Ying Wang,[†] Yujin Chen,*[,‡] Longqiang Wang,[†] Shaoqiang Yang,[†] Guorui Chen,[†] Guobao Li,*[,§] Yuzeng Sun,[§] and Wei Qin*[,$]

[†]Key Laboratory of Superlight Materials and Surface Technology, Ministry of Education, and [‡]College of Science, Harbin Engineering University, Harbin, Heilongjiang, 150001, China

[§]Beijing National Laboratory for Molecular Sciences, State Key Laboratory of Rare Earth Materials Chemistry and Applications, Peking University, Beijing 100871, China

[$]School of Materials Science and Engineering, Harbin Institute of Technology, Harbin 150001, China

Supporting Information

ABSTRACT: Anatase TiO_2 nanobelts with 13 nm in thickness have been successfully synthesized via an epitaxial growth chemical transformation, in which the primary $H_2Ti_3O_7$ nanobelt frameworks can be preserved. The phases, crystal structures, morphologies, and growth behavior of both the precursory ($Na_2Ti_3O_7$ and $H_2Ti_3O_7$) and resultant products (TiO_2) are characterized by powder X-ray diffraction (XRD), scanning electron microscopy (SEM), transmission electron microscopy (TEM), and selected area electron diffraction (SAED). Detailed investigation of the formation mechanism of the TiO_2 nanobelts indicates epitaxial nucleation and oriented growth of textured TiO_2 inside the nanobelts. TiO_2 nanocrystals prefer certain epitaxial growth direction due to the structural matching of $(110)_{H2Ti3O7}//(101)_{TiO2}$. We demonstrated that the initial reversible capacity of these TiO_2 nanobelts attained 225 mA h/g. Furthermore, the nanobelts exhibit high power density along with excellent cycling stability in their application as hybrid electrochemical cells.

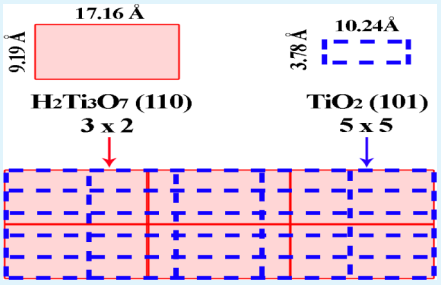

KEYWORDS: *epitaxial growth, Anatase, $H_2Ti_3O_7$ nanobelts, TiO_2 nanobelts, electrochemical performance, lithium-ion batteries*

INTRODUCTION

Titanium dioxide (TiO_2) is an important class of n-type semiconducting materials that shows interesting characteristics, such as photocatalysis,[1−4] solar cell,[5−8] electrochemistry,[9−12] biology,[13−15] and gas sensors.[16−18] Significantly, TiO_2 is of lower cost, no toxicity, and high chemical stability in comparison with other metal oxides such as SnO_2 and ZnO that have been commonly studied. Now, inexpensive, nontoxic stoichiometric TiO_2 is considered an attractive candidate as an anode for rechargeable lithium-ion batteries (LIBs) because it is an efficient, low-voltage intercalation host for lithium ions.[19−21] Among the TiO_2 polymorphs, anatase,[21−23] rutile,[24] brookite,[25] and bronze (TiO_2−B) were applied for LIBs.[20]

It is well-known that the chemical compositions, polymorphs, and morphologies such as crystallite sizes, shapes, orientations, and assemblies, which are related to the preparation methodology, would have a significant influence on the performances of as prepared metal oxides.[26,27] To develop new functional materials with enhanced performance, the rational design and preparation of nanostructured materials has been continuously pursued. For TiO_2, there has been a growing endeavor in the synthesis and applications of nanostructured materials. Many synthesis approaches have been recently achieved, for example electron beam evaporation,[28] low-temperature oxidation,[29] chemical vapor deposition,[30,31] physical vapor deposition,[32] dip coating,[33] spin coating,[34] atmosphere pressure chemical vapor deposition and the sol−gel method.[35,36] In addition, nanostructured TiO_2 based materials (e.g., nanoparticles,[37] nanotubes,[38] nanofibers,[39] and nanoporous structures[40]) are currently receiving much attention because of their unique chemical, electronic and catalytic properties. In addition, it is desirable to develop novel methods to produce new oriented TiO_2-based nanomaterials both in large quantities and inexpensively. Uniform titania nanotube arrays have been prepared via anodic oxidation of titanium in a hydrofluoric (HF) electrolyte.[41,42] The controlled sol−gel synthesis of titania, in particular in combination with block copolymer templates, was also a promising method for highly organized and oriented mesoporous titania.[43,44] A electrospinning technique has been applied for generating nanofibers of anatase TiO_2 with controllable diameters and porous structures.[45] According to the reported literature, it was found that the most precursors for 1D nanostructured titanate and TiO_2 materials were TiO_2 powders or $Ti(OC_3H_7)_4$.[46−51] It was also found that metal Ti could act as the precursor for obtaining $Na_2Ti_6O_{13}$, $H_2Ti_3O_7$ and TiO_2.[52] However, the exact

Received: October 17, 2012
Accepted: December 24, 2012
Published: December 24, 2012

growing mechanism form $H_2Ti_3O_7$ to TiO_2 in literatures was not clarified. In addition, in our work, using metal Ti as the precursor, it was found that different titanate ($Na_2Ti_3O_7$) was obtained, not $Na_2Ti_6O_{13}$.

Herein, we report the fabrication of unique crystalline TiO_2 nanobelts by a thermal decomposition from precursory $H_2Ti_3O_7$ nanobelts based on the epitaxial growth relationship between the $(110)_{H2Ti3O7}$ and $(101)_{TiO2}$ planes. During the formation of crystalline TiO_2, the nanobelt frameworks (skeletons) could be maintained, as was expected on the basis of previous work involving single-crystalline TiO_2 nanosheets.[53] This epitaxial growth will provide an effective and versatile route to controlled fabrication of nanostructured oxides with optimizable properties. The electrochemical performance of the TiO_2 nanobelts as anode in Li-ion batteries will be presented.

EXPERIMENTAL SECTION

Synthesis of the Precursor. All of the chemicals were of analytical grade and were used as received. Titanate nanobelts were prepared by hydrothermal reaction of titanium powders with a NaOH aqueous solution. In a typical experiment, about 0.4 g of titanium powders was dispersed in 36 mL of 10 M NaOH aqueous solution. After sonication in an ultrasonic bath for 30 min, the solution was transferred to a 50 mL Teflon lined stainless autoclave. The autoclave was maintained at 205 °C under autogenous pressure for 24 h and then cooled to room temperature naturally. The purpose of the ultrasonic treatment is to make the titanium powder better dispersed and wetted in the solution. The reaction product was washed with distilled water until a pH value of about 7 was reached to get sodium titanate nanobelts. The obtained sodium titanate nanobelts were treated with a solution of 0.1 M HCl for 10h, and then rinsed with deionized water several times until a pH value of about 7 was reached. The washed samples were dried at 80 °C for 24 h and hydrogen titanate nanobelts were produced.

Preparation of TiO_2 Nanobelts. In a typical preparation of TiO_2 nanobelts, the as-synthesized $H_2Ti_3O_7$ precursor was converted into pure TiO_2 phase by calcination. The typical heating process was carried out in a crucible without using any inert gases for protection, and the temperature was increased up to 500 °C at 10 °C/min, and then maintained for 2.0 h.

Characterization. The as-prepared samples were characterized by an X-ray diffractometer (XRD) on a Rigaku X-ray Diffractometer with graphite monochromatized Cu−Kα radiation (λ = 1.54178 Å). Scanning electron microscopy (SEM) images were taken with a JEOL-5600LV scanning electron microscope, using an accelerating voltage of 20 kV. The high-resolution transmission electron microscopic (HRTEM) image and selected area electron diffraction (SAED) of the nanobelts were taken with a JEOL HRTEM (JEM2010 electron microscope) with 200 kV accelerating voltage.

Electrochemical Performance. For the electrochemical measurements, the as-prepared TiO_2 samples were mixed with acetylene black and polyvinylidene fluoride (PVDF) at a weight ratio of 75:15:10 in N-methyl-2-pyrrolidene (NMP) solution. The dried material was coated on a copper foil and dried in a vacuum oven at 130 °C for 10 h and was pressed and then cut into a disc of 1 cm^2. The 2016 coin-type cells were assembled in an argon filled glovebox using pure lithium as the counter electrode, 1 M $LiClO_4$ [ethylene carbonate (EC): dimethylcarbonate (DMC) = 1:1 in volume] as the electrolyte, and a microporous membrane (Celguard 2400, USA) as the separator. The cells were galvanostatically charged and discharged between 0.0 and 3.0 V versus Li^+/Li at room temperature (25 °C) on a program-controlled test system (CT2001, Land Battery Co., China).

RESULTS AND DISCUSSION

$Na_2Ti_3O_7$ Precursor Nanobelts. The reaction of titanium powders and a NaOH aqueous solution at 205 °C can yield layered monoclinic-structured $Na_2Ti_3O_7$. The X-ray diffraction (XRD) pattern of the as-synthesized product exhibits an intense and sharp diffraction peak at ca. 10.5° (Figure 1a),

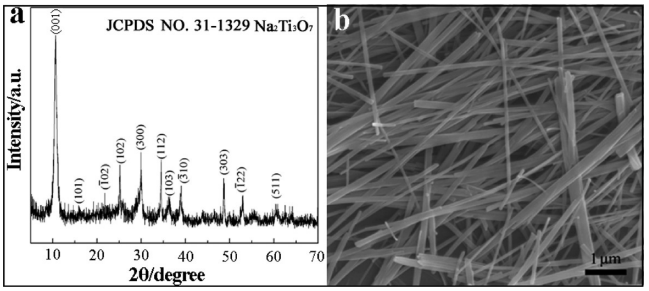

Figure 1. (a) XRD pattern and (b) SEM image of the as-prepared $Na_2Ti_3O_7$ nanobelts.

which is assigned to the (001) reflection of monoclinic $Na_2Ti_3O_7$ ($P2_1/m$, PCPDF 31−1329), indicative of highly oriented growth. Besides the (001) reflection, a successive strong (300) reflection appears with a relative d-spacing of 2.98 Å. And its average crystallite size calculated by the Scherrer-equation is 15.7 nm. The morphology of the as-synthesized $Na_2Ti_3O_7$ nanobelts is examined by scanning electron microscopy (SEM). Figure 1b shows the SEM image of the typical product grown at 205 °C for 24 h. The nanobelts have extraordinarily smooth surfaces, and their typical size is in the range of 20−50 nm in thickness, ~ 200 in widths, and up to 10 μm in length. It is clear that the $Na_2Ti_3O_7$ nanobelts have a highly oriented growth behavior and fairly high aspect ratio, which may improve their physicochemical properties, thus enhancing their practical applications.

$H_2Ti_3O_7$ Precursor Nanobelts. The as-obtained $Na_2Ti_3O_7$ nanobelts were acidized with a 0.1 M HCl solution and transformed into $H_2Ti_3O_7$ nanobelts with similar sizes and morphology, as shown in Figure 2a. XRD patterns (Figure 2b) of the products acidized for different times (2h, 4h, 6h, 8h and 10h) confirms that the complete transformation from monoclinic $Na_2Ti_3O_7$ to monoclinic $H_2Ti_3O_7$ needs only two

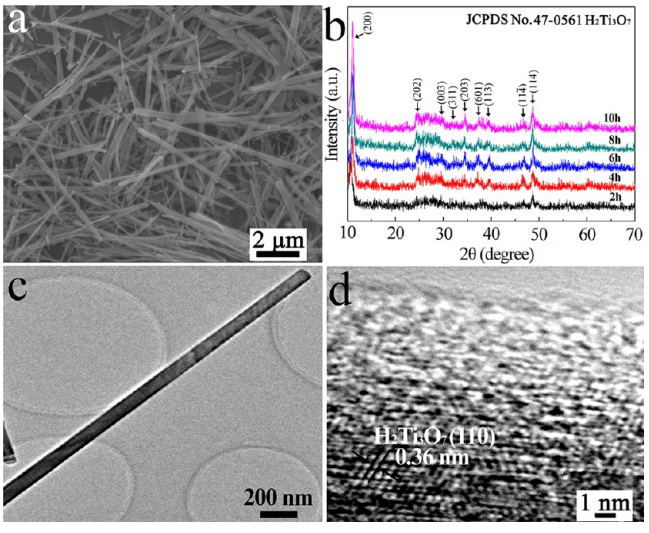

Figure 2. (a, c, d) SEM, TEM, and HRTEM images of the as-prepared $H_2Ti_3O_7$ nanobelts acidized for 10 h; (b) XRD patterns of as-obtained products with different acidation times.

dx.doi.org/10.1021/am302366h | ACS Appl. Mater. Interfaces 2013, 5, 368−373

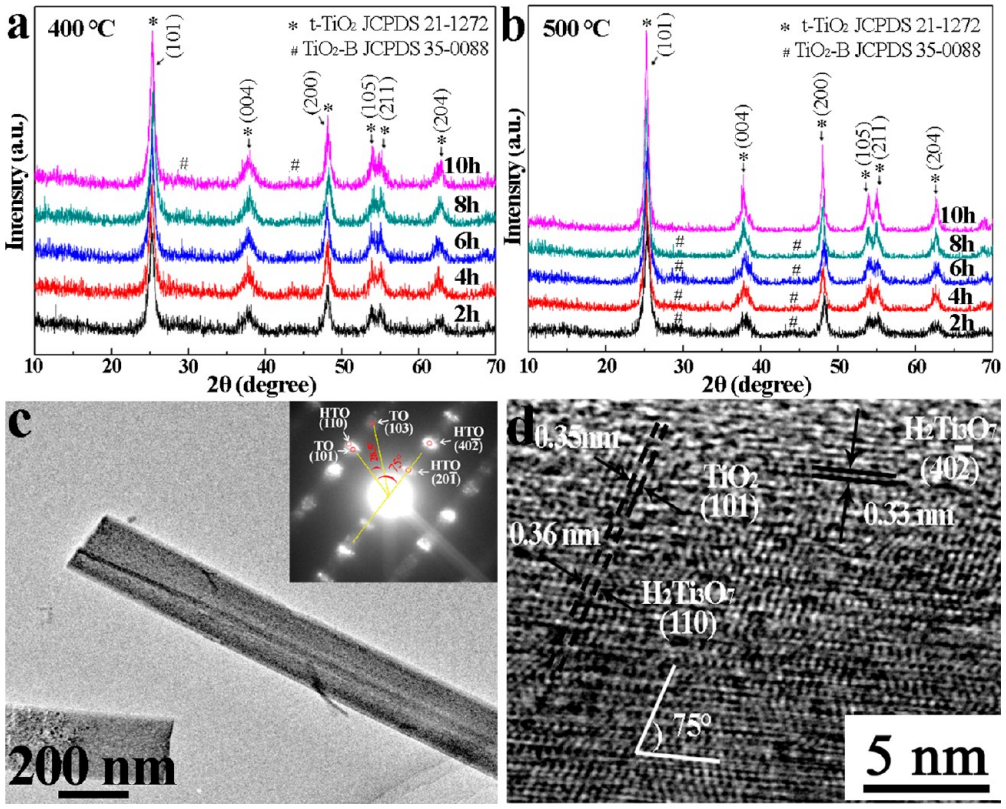

Figure 3. (a, b) XRD patterns of the products with different calcinations' times; (c, d) TEM, HRTEM images and SAED pattern of the product obtained by thermal decomposition of $H_2Ti_3O_7$ nanobelts at 500 °C for 0.2 h.

hours. And their average crystallite sizes calculated by the Scherrer-equation are about 8.8 nm (2 h), 10.5 nm (4 h), and 11 nm (6−10 h), respectively. The structure and growth behavior of the $H_2Ti_3O_7$ nanobelts are further investigated by TEM and HRTEM. Figure 2c displays a microtomed cross-section TEM image of an $H_2Ti_3O_7$ nanobelt, which provides a top-view.

The relevant HRTEM image as shown in Figure 2d indicates a highly crystalline character with a considerably distinct lattice spacing of 0.36 nm that corresponds to the value of the (110) planes.

Thermal Decomposition of $H_2Ti_3O_7$. Layered hydrogen titanate would be converted to TiO_2−B, anatase (t-TiO_2), or rutile polymorph with the increasing of calcination temperatures.[54] The crystal structural transformation from $H_2Ti_3O_7$ to TiO_2 has been studied in details by in situ XRD in air at various temperatures from 400 to 500 °C, which has been widely reported as the key conversional temperature area in literatures. As shown in Figure 3a, all the products calcined at 400 °C for different times are mixtures of TiO_2−B and anatase TiO_2. And their average crystallite sizes calculated by the Scherrer-equation are about 12.5 nm (2 h) and 15 nm (4−10 h), respectively. But at 500 °C, phase-pure anatase TiO_2 can be obtained after 10 h aging (Figure 3b), whose average crystallite sizes calculated by the Scherrer-equation are about 14 nm (2−6 h), 18 nm (8 h), and 20 nm (10 h), respectively. It is clear that the $H_2Ti_3O_7$ nanobelts are quickly converted into anatase TiO_2 nanobelts calcined at 400 or 500 °C. It is also found in the above patterns that the XRD peaks slightly shift to right, which implies a shrinkage process of the lattice parameters. After thermal decomposition of $H_2Ti_3O_7$ nanobelts at 500 °C for 2 h, anatase TiO_2 appears, which can be further identified in the HRTEM images c and d in Figure 3. Interestingly, HRTEM result indicates that the heterostructured nanobelt is composed of parallel segment of monoclinic $H_2Ti_3O_7$ and anatase TiO_2, which reveals the epitaxial relationship, $H_2Ti_3O_7$ (110) matching TiO_2 (101). And the SAED result containing their diffraction points also confirms the above conclusion, as shown in Figure 3c inset and Figure S1 in the Supporting Information.

Crystalline Anatase TiO_2 Nanobelts. Subsequent thermal treatment in air was carried out at 500 °C temperatures for 2−10 h. With increasing aging time to 10 h, highly crystalline t-TiO_2 is obtained (Figure 3b). In addition, no peaks of other phases were detected, indicating that the calcined samples are of high purity. SEM images show retentive nanobelt morphology characteristics of the products prepared at 500 °C for 2−10 h (Figure 4), which indicates the stability of $H_2Ti_3O_7$ nanobelt frameworks. Further observation of the nanobelts reveals that the nanobelts are much rougher, slightly shrunken, and shorter with the thermal decomposition times prolonging, which may be due to a recrystallization process.

Using the as-grown $H_2Ti_3O_7$ nanobelts as a precursor, pure t-TiO_2 nanobelts could be prepared via a thermal treatment of $H_2Ti_3O_7$ in air (Figures 3b and 4e). Further structural characterization was performed for the sample prepared at 500 °C for 10 h by HRTEM and SAED measurements (Figure 5).

The SAED pattern in Figure 5a confirms the highly oriented growth of TiO_2 nanobelts and crystal-like nature. The distinct lattice stripes in HRTEM image (Figure 5b) reveals the wall of a TiO_2 nanobelt is well crystallized.

Epitaxial Growth Mechanism. The formation mechanism of TiO_2 is via an epitaxial growth process, which involves dissolution−crystallization process. Titanium particle precursor

dx.doi.org/10.1021/am302366h | ACS Appl. Mater. Interfaces 2013, 5, 368−373

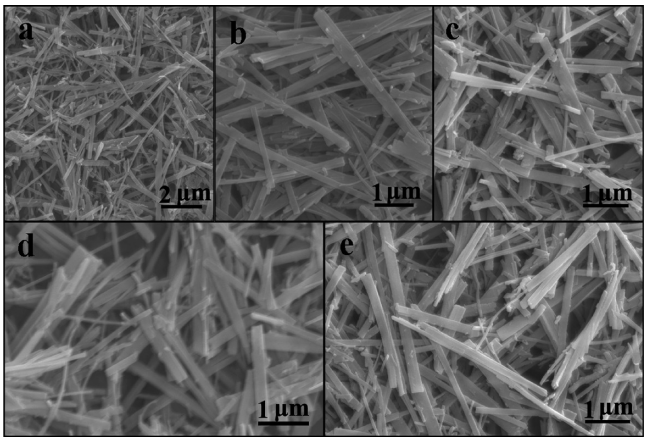

Figure 4. SEM images of the products obtained by thermal decomposition of $H_2Ti_3O_7$ nanobelts at 500 °C for different times: (a) 2, (b) 4, (c) 6, (d) 8, and (e) 10 h.

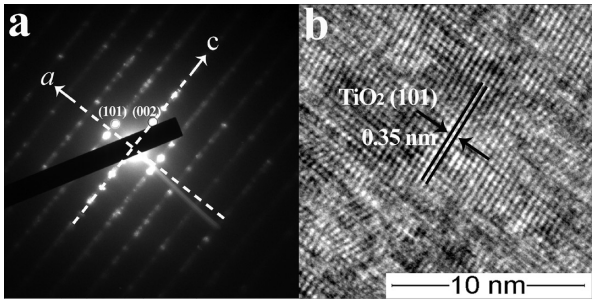

Figure 5. SAED and HRTEM image of the as-prepared t-TiO_2 nanobelt.

is initially dissolved and hydrolyzed into titanate under the hydrothermal reaction. During the alkali hydrothermal reaction, the titanium particle reacts with high concentration NaOH to form sodium titanate. Subsequently, the sodium titanate is washed with HCl to form hydrogen titanate and byproduct sodium chloride. The Na^+ cations distributing in the interspacing of the octahedral titanium complexes can be substituted with H^+ cations by ion exchange when sodium titanate is immersed in HCl for a sufficient time, as reported in the literature.[55] Anatase titania then is obtained under dehydration process at 500 °C. The entire chemical process that takes place is as follows:

$$3Ti + 2NaOH + 3O_2 \rightarrow Na_2Ti_3O_7 + H_2O \quad (1)$$

$$Na_2Ti_3O_7 + 2HCl \rightarrow H_2Ti_3O_7 + 2NaCl \quad (2)$$

$$H_2Ti_3O_7 \rightarrow 3TiO_2 + H_2O \quad (3)$$

Thus, upon oxidation of titanium particles using NaOH and adequate acid washing (by ion exchange), metal Ti is conversed to form "Ti−O frame work"—titanate and anatase titania. It is noted that the titanate and anatase titania have a common structural features, with crystal lattices consisting of the octahedra sharing four edges and the zigzag chain-like structure.[55] These chains are joined together by sharing edges to form layers and protons or Na^+ ions can be incorporated between the layers. The distance between the layers is variable, which resulted in the high flexibility of these high aspect ratio nanostructures. In the reaction with the acid, the zigzag chainlike structural units of TiO_2 nanobelts remain relatively unchanged other than lattice rotation and rearrangement of the $[TiO_6]$ octahedra to form anatase lattice.[56] Thus, it is postulated that anatase titania phase formed on the basis of the parent titanate nanostructures. It is interesting to note that the produced titania and hydrogen titanate nanostructures retain essentially the similar morphologies and interplanar crystal spacings (0.35 and 0.36 nm) made of same angles with the nanobelt's axial lead, as shown in Figure 3d. In the figure the spacings between the parallel fringes are correspond to the (101) and (110) lattice planes of TiO_2 and $H_2Ti_3O_7$, respectively. Thus, the $TiO_2/H_2Ti_3O_7$ nanobelts are determined as epitaxial growth with the relationship of $(110)_{H2Ti3O7}//(101)_{TiO2}$. This interesting nanomaterial that single nanobelt is composed of parallel segment of TiO_2 and $H_2Ti_3O_7$ has not been found in previous literatures. The possible lattice matching relationship has been illustrated in the following Scheme 1. This observation confirms that the

Scheme 1. Schematic Diagram of the Lattice Matching Relationship between Titania and Hydrogen Titanate Phase in the Epitaxial Growth Process

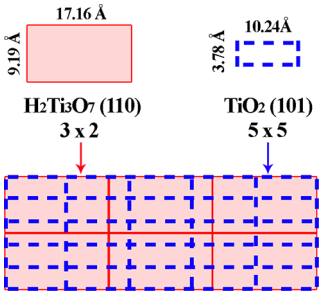

hydrogen titanate structural host motifs are easily intercalated with H^+ with slight lattice rotation and rearrangement of crystal structures without modifying its final morphology. The above detailed structural measurements and analysis have proved the epitaxial growth mechanism adequately.

Anatase TiO_2 Nanobelts' Electrochemical Performance. In this work, the feasibility of TiO_2 nanobelts for use in lithium electrochemical insertion has also been explored. As shown in Figure 6a, the first discharge capacities of the products calcined at 500 °C for different times (2−10 h) are 193, 200, 211, 216, and 225 mA h/g at a current density of 30 mA/g, respectively. It is obvious that pure t-TiO_2 has bigger discharge capacity than other nanobelts containing $H_2Ti_3O_7$ or TiO_2−B. After 50 cycles, the discharge capacity of the as-synthesized pure TiO_2 nanobelts by thermal decomposition of $H_2Ti_3O_7$ nanobelts at 500 °C for 10 h is still over 210 mA h/g, as shown in Figure 6b. During the first discharge (Li insertion), a total capacity of 225 mA h/g is achieved at the end of the first discharge with a final reversible capacity of 210 mAh/g, leading to an irreversible capacity of 15 mA h/g. In Figure 6a, the potential of discharge curve rapidly drops to a well-defined plateau at 1.7 V associated with the intercalation of Li^+ through two phase equilibrium of a Li-poor (tetragonal) and a Li-rich (orthorhombic) phase. The main reason for the capacity drop during the first discharge/charge cycles is that a small part of the insertion/extraction of Li^+ into/from TiO_2 nanotubes is irreversible, which should be related to the size, morphology, crystallinity of the as-synthesized samples. The loss of capacity may also be due to the formation of a thin surface film at the electrode surface and irreversible reaction of Li^+ with traces of

dx.doi.org/10.1021/am302366h | ACS Appl. Mater. Interfaces 2013, 5, 368−373

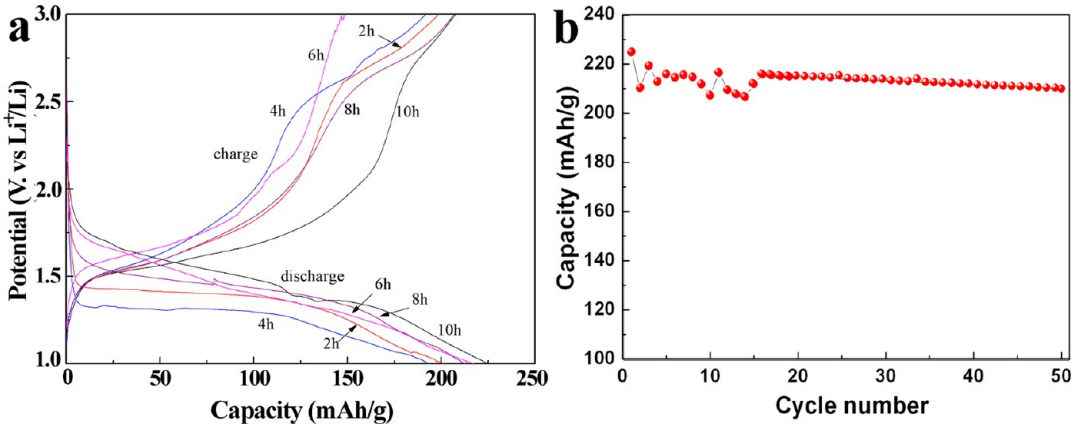

Figure 6. (a) First potential−capacity profiles at the charge/discharge current density of 30 mA/g of the nanobelt products obtained by thermal decomposition of $H_2Ti_3O_7$ nanobelts at 500 °C for different times (2, 4, 6, 8, and 10 h); (b) cycle life of the as-synthesized pure TiO_2 nanobelts by thermal decomposition of $H_2Ti_3O_7$ nanobelts at 500 °C for 10 h.

water.[57] The Li-ion insertion/extraction reaction in TiO_2 nanotube electrodes can be written as

$$xLi^+ + xe^- + TiO_2 \leftrightarrow Li_xTiO_2 \quad (4)$$

The insertion coefficient, x, in anatase is usually close to 0.5.[58] The first lithium insertion max capacity of products calcined at 500 °C is observed to be 225 mA h/g, corresponding to the lithium insertion coefficient of 0.67. The larger capacity obtained may be ascribed to a shorter diffusion length for both the electron and Li^+ and a larger electrode/electrolyte contact area of TiO_2 nanobelts compared with traditional materials, which facilitate the lithium ions' insertion and extraction. Further investigation of its capacities at the different charge/discharge current density (30 mA/g to 240 mA/g) indicated that their capacities reduced quickly, even down to several mA h/g, as shown in Figure S2 in the Supporting Information.

CONCLUSIONS

In conclusion, we report an epitaxial growth transformation route to anatase TiO_2 nanobelts with highly textured nanowalls from smooth $H_2Ti_3O_7$ nanobelts. The epitaxial growth conversation is based on the structural matching of $(110)_{H2Ti3O7}//(101)_{TiO2}$. During the chemical and structural change from $H_2Ti_3O_7$ to TiO_2, the nanobelt morphology can be preserved. The epitaxial growth provides a rational and effective approach to prepare highly organized 1D nanomaterials. The result of galvanostatic cycling measurement in the voltage range of 0.0−3.0 V versus Li^+/Li at 30 mA/g give reversible capacities of 210 mA h/g for the pure TiO_2 nanobelts calcined at 500 °C, which shows high capacitance and stable reversibility, indicative of microstructure optimized performance.

ASSOCIATED CONTENT

Supporting Information

Enlarged SAED analysis determining the epitaxial relationship between TiO_2 (TO) and $H_2Ti_3O_7$ (HTO); the capacities at the different charge/discharge current density (30 mA/g to 240 mA/g) of the as-synthesized pure TiO_2 nanobelts by thermal decomposition of $H_2Ti_3O_7$ nanobelts at 500 °C for 10 h. This material is available free of charge via the Internet at http://pubs.acs.org.

AUTHOR INFORMATION

Corresponding Author

*E-mail: gaopeng@hrbeu.edu.cn.

Notes

The authors declare no competing financial interest.

ACKNOWLEDGMENTS

We thank the Program for NCET in University (NECT-10-0049), the Natural Science Foundation of China (Grant 21001035, 51272050, and 51072038); the Specialized Research Fund for the Doctoral Program of Higher Education of China (No. 20092304120021); Harbin key Sci-tech project (2010AA4BG004); the Fundamental Research funds for the Central Universities (HEUCF201210006 and HEUCFT1010) and Outstanding Youth Foundation of Heilongjiang Province (Grant JC201008) for the financial support of this research.

REFERENCES

(1) Williams, G.; Seger, B.; Kamat, P. V. *ACS Nano* **2008**, *2*, 1487−1491.
(2) Wu, N. Q.; Wang, J.; Tafen, D. N.; Wang, H.; Zheng, J. G.; Lewis, J. P.; Liu, X. G.; Leonard, S. S.; Manivannan, A. *J. Am. Chem. Soc.* **2010**, *132*, 6679−6685.
(3) Linsebigler, A. L.; Lu, G. Q.; Yates, J. T. *Chem. Rev.* **1995**, *95*, 735−758.
(4) Osterloh, F. E. *Chem. Mater.* **2008**, *20*, 35−54.
(5) Bach, U.; Lupo, D.; Comte, P.; Moser, J. E.; Weissortel, F.; Salbeck, J.; Spreitzer, H.; Gratzel, M. *Nature* **1998**, *395*, 583−585.
(6) O'Regan, B.; Grätzel, M. *Nature* **1991**, *353*, 737−740.
(7) Shankar, K.; Feng, X. J.; Grimes, C. A. *ACS Nano* **2009**, *3*, 788−794.
(8) Bang, J. H.; Kamat, P. V. *ACS Nano* **2009**, *3*, 1467−1476.
(9) Guo, Y. G.; Hu, Y. S.; Sigle, W.; Maier, J. *Adv. Mater.* **2007**, *19*, 2087−2091.
(10) Hu, Y. S.; Kienle, L.; Guo, Y. G.; Maier, J. *Adv. Mater.* **2006**, *18*, 1421−1426.
(11) Kim, S. W.; Han, T. H.; Kim, J.; Gwon, H.; Moon, H. S.; Kang, S. W.; Kim, S. O.; Kang, K. *ACS Nano* **2009**, *3*, 1085−1090.
(12) Meekins, B. H.; Kamat, P. V. *ACS Nano* **2009**, *3*, 3437−3446.
(13) Paunesku, T.; Rajh, T.; Wiederrecht, G.; Maser, J.; Vogt, S.; Stojicevic, N.; Protic, M.; Lai, B.; Oryhon, J.; Thurnauer, M.; Woloschak, G. *Nat. Mater.* **2003**, *2*, 343−346.
(14) Magrez, A.; Horváth, L.; Smajda, R.; Salicio, V.; Pasquier, N.; Forró, L.; Schwaller, B. *ACS Nano* **2009**, *3*, 2274−2280.
(15) Mun, K. S.; Alvarez, S. D.; Choi, W. Y.; Sailor, M. J. *ACS Nano* **2010**, *4*, 2070−2076.

(16) Garzella, C.; Comini, E.; Tempesti, E.; Frigeri, C.; Sberveglieri, G. *Actuators B* **2000**, *68*, 189−196.
(17) Carotta, M. C.; Ferroni, M.; Gnani, D.; Guidi, V.; Merli, M.; Martinelli, G.; Casale, M. C.; Notaro, M. *Sens. Actuators B* **1999**, *58*, 310−317.
(18) Radecka, M.; Zakrzewska, K.; Rekas, M. *Sens. Actuators B* **1998**, *47*, 194−204.
(19) Armstrong, A. R.; Armstrong, G.; Canales, J.; Garcia, R.; Bruce, P. G. *Adv. Mater.* **2005**, *17*, 862−865.
(20) Yang, Z. G.; Choi, D.; Kerisit, S.; Rosso, K. M.; Wang, D. H.; Zhang, J.; Graff, G.; Liu, J. *J. Power Sources* **2009**, *192*, 588−598.
(21) Chen, J. S.; Tan, Y. L.; Li, C. M.; Cheah, Y. L.; Luan, D. Y.; Madhavi, S.; Boey, F. Y. C.; Archer, L. A.; Lou, X. W. *J. Am. Chem. Soc.* **2010**, *132*, 6124−6130.
(22) Cava, R. J.; Murphy, D. W.; Zahurak, S.; Santoro, A.; Roth, R. S. *J. Solid State Chem.* **1984**, *53*, 64−75.
(23) Olson, C. L.; Nelson, J.; Islam, M. S. *J. Phys. Chem. B* **2006**, *110*, 9995−10001.
(24) Ohzuku, T.; Takehara, Z.; Yoshizawa, S. *Electrochim. Acta* **1979**, *24*, 219−222.
(25) Reddy, M. A.; Kishore, M. S.; Pralong, V.; Varadaraju, U. V.; Raveau, B. *Electrochem. Solid-State Lett.* **2007**, *10*, 29−31.
(26) Feng, J.; Zeng, H. C. *Chem. Mater.* **2003**, *15*, 2829−2835.
(27) He, L.; Chen, C. P.; Wang, N.; Zhou, W.; Guo, L. *J. Appl. Phys.* **2007**, *102*, 103911−103914.
(28) Yang, T. S.; Shiu, C. B.; Wong, M. S. *Surf. Sci.* **2004**, *548*, 75−82.
(29) Lee, K. S.; Park, I. S. *Scr. Mater.* **2003**, *48*, 659−663.
(30) Marco de Lucas, M. C.; Fabreguette, F.; Collin, S.; Bourgeois, S. *Int. J. Inorg. Mater.* **2000**, *2*, 255−259.
(31) Byun, D.; Jin, Y.; Kim, B.; Lee, J. L.; Park, D. *J. Hazard. Mater. B* **2000**, *73*, 199−206.
(32) Damiriv, D.; Bally, A. R.; Ballif, C.; Homes, P.; Schmid, P. E.; Sanjines, R.; Levy, F.; Parvulescu, V. I. *Appl. Catal., B* **2000**, *25*, 83−92.
(33) Wang, X. P.; Yu, Y.; Hu, X. F.; Gao, L. *Thin Solid Films* **2000**, *371*, 148−152.
(34) Kato, K.; Tsuzuki, A.; Taoda, H.; Torrii, Y.; Kato, T.; Batsugn, Y. *J. Mater. Sci.* **1994**, *29*, 5911−5915.
(35) Liu, S. M.; Gan, L. M.; Lu, L. H.; Zhang, W. D.; Zheng, H. C. *Chem. Mater.* **2002**, *14*, 1391−1397.
(36) Burnside, S. D.; Shklower, V.; Barbe, C.; Comte, P.; Arendse, F.; Brookes, K.; Grätzel, M. *Chem. Mater.* **1998**, *10*, 2419−2425.
(37) Wang, C. Y.; Groenzin, H.; Shultz, M. J. *J. Phys. Chem. B* **2004**, *108*, 265−272.
(38) Tian, Z. R. R.; Voigt, J. A.; Liu, J.; Mckenzie, B.; Xu, H. F. *J. Am. Chem. Soc.* **2003**, *125*, 12384−12385.
(39) Yoo, S.; S. Akbar, A.; Sandhage, K. H. *Adv. Mater.* **2004**, *16*, 260−264.
(40) Yang, P.; Zhao, D.; Margolese, D. I.; Chmelka, B. F.; Stucky, G. D. *Nature* **1998**, *396*, 152−154.
(41) Gong, D.; Grimes, C. A.; Varghese, O. K.; Hu, W.; Singh, R. S.; Chen, Z.; Dickey, E. C. *J. Mater. Res.* **2001**, *16*, 3331−3334.
(42) Mor, G. K.; Varghese, O. K.; Paulose, M.; Shankar, K.; Grimes, C. A. *Sol. Energy Mater. Sol. Cells* **2006**, *90*, 2011−2075.
(43) Crepaldi, E. L.; Soler-Illia, G. J.; Grosso, D.; Grosso, D.; Cagnol, F.; Ribot, F.; Sanchez, C. *J. Am. Chem. Soc.* **2003**, *125*, 9770−9786.
(44) Rawolle, M.; Niedermeier, M. A.; Kaune, G.; Perlich, J.; Lellig, P.; Memesa, M.; Cheng, Y. J.; Gutmann, J. S.; Muller-Buschbaum, P. *Chem. Soc, Rev.* **2012**, *41*, 5131−5142.
(45) Li, D.; Xia, Y. N. *Nano Lett.* **2003**, *3*, 555−560.
(46) Shim, H. W.; Lee, D. K.; Cho, I. S.; Hong, K. S.; Kim, D. W. *Nanotechnology* **2010**, *21*, 255706.
(47) Wang, Y.; Du, G.; Liu, H.; Liu, D.; Qin, S.; Wang, N.; Hu, C.; Tao, X.; Jiao, J.; Wang, J.; Wang, Z. *Adv. Funct. Mater.* **2008**, *18*, 1131−1137.
(48) Kim, J.; Cho, J. *J. Electrochem. Soc.* **2007**, *154*, A542−546.
(49) Wang, H.; Kuo, C.; Lin, H.; Kuo, I.; Cheng, C. *J. Am. Ceram. Soc.* **2006**, *89*, 3388−3392.
(50) Bavykin, D. V.; Friedrich, J. M.; Walsh, F. C. *Adv. Mater.* **2006**, *18*, 2807−2824.
(51) FEIST, T. P.; DAVIES, P. K. *J. Solid State Chem.* **1992**, *101*, 275−295.
(52) Peng, X.; Chen, A. *Adv. Funct. Mater.* **2006**, *16*, 1355−1362.
(53) Wen, P. H.; Ishikawa, Y.; Itoh, H.; Feng, Q. *J. Phys. Chem. C* **2009**, *113*, 20275−20280.
(54) Finnegan, M. P.; Zhang, H. Z.; Banfield, J. F. *J. Phys. Chem. C* **2007**, *111*, 1962−1968.
(55) Wei, M.; Konishi, Y.; Zhou, H.; Sugihara, H.; Arakawa, H. *Chem. Phys. Lett.* **2004**, *400*, 231−234.
(56) Zhu, H.; Lan, Y.; Gao, X.; Ringer, S. P.; Zheng, Z.; Song, D.; Zhao, J. *J. Am. Chem. Soc.* **2005**, *127*, 6730−6736.
(57) Jung, J. H.; Kobayashi, H.; Van Bommel, K. J. C.; Shinkai, S.; Shimizu, T. *Chem. Mater.* **2002**, *14*, 1445−1447.
(58) Kavan, L.; Gratzel, M.; Rathousky, J.; Zukal, A. *J. Electrochem. Soc.* **1996**, *143*, 394−400.